Supporting Information for

Salt Fingers Contribute Substantially to Diapycnal Oxygen Transport into the Oxygen Minimum Zone of the Eastern South Pacific

Pinto-Juica M.[12], et al., 2025

Contents of this file

Introduction

This material is included to complement the main text by detailing:

1. The methodology used to analyze the winds during the different field campaigns in terms of upwelling conditions.
2. World Ocean Data set used in the study and processing.
3. Underwater glider data processing.
4. Methodological details about estimations of the dissipation rates ε and χ methods.
5. Salt fingers identification and diapycnal diffusivity calculation methods.

Note 1: Wind Conditions for Each Field Campaign

The wind conditions before and during each field campaign were assessed using hourly wind data from the ERA5 hourly product (Hersbach et al., 2020), which has a spatial resolution of 0.25°x0.25°. The closest grid point to the mean position of the stations was selected to characterize the region in terms of upwelling and downwelling conditions.

The alongshore wind stress (favorable to upwelling or downwelling in the region) was calculated from ERA5 wind data as:

$$\tau_v = \rho_a C_d v_{10} U_{10} \tag{S1}$$

where v_{10} is the meridional wind velocity vector at 10 m above sea level, which in our study area is in good alignment with the coast, so is considered as the alongshore component for Ekman dynamics purpose (see Figure 1 in the main text), ρ_a = 1.225 kg m^{-3} is the air density, C_d is the adimensional drag coefficient, and U_{10} is the wind magnitude. The drag coefficient was computed following Yelland & Taylor, 1996:

$$10^3 C_d = 0.29 + \frac{3.1}{U_{10}} + \frac{7.7}{U_{10}^2}, for\ U_{10} \leq 6ms^{-1} \tag{S2}$$

$$10^3 C_d = 0.60 + 0.07U_{10}, for\ 6ms^{-1} \leq U_{10} \tag{S3}$$

The characterization of each campaign was done using the wind impulse (I(t)) derived from the meridional wind stress, calculated following Cushman-Roisin & Beckers (2011):

$$I(t) = \int_{T1}^{T2} \tau_v(t)dt \tag{S4}$$

where τ_v is the meridional wind stress and T1 and T2 are the beginning and end of the wind event characterization, which are defined here as T1 = 5 days before the first measurements set and T2 = 2 days after.

Note 2: CTD Data from the World Ocean Data Base

Hydrographic data from the World Ocean Database (WODB) spanning 1980–2022 were used to characterize the major Oxygen Minimum Zones (OMZs) globally, including the Peru–Chile, California, Benguela, and Canary systems (Figure S2a–d). All available profiles within a 2.5° offshore band from the coastline were included in the analysis. Conservative temperature, absolute salinity, and dissolved oxygen profiles were linearly interpolated at 10 m intervals between 100 and 1000 m.

To construct alongshore sections, data were averaged within grid cells of 2.5° longitude × 0.5° latitude for each OMZ domain and subsequently linearly interpolated to generate the composite transects shown in Figure 3b (main text) and Figures S3a–c. Turner angles were computed using the TEOS-10 toolbox routines (McDougall & Barker, 2011; Feistel, 2012).

Note 3: Turner angles from underwater glider transects along 36.5°S

Data from eight glider transects conducted near 36.5°S between 2010 and 2012, spanning from the coast to approximately 180 km offshore (see Figure 1a, main text), were used to estimate Turner angles (Tu) in the study region. The glider datasets included conservative temperature, absolute salinity, and dissolved oxygen (see Figures S4a–c; see also Figures 3c and 3d, main text), along with other variables not shown here. Details on glider operation and data processing are provided in Pizarro et al. (2016).

For visualization, the data were interpolated onto a regular grid extending from the coast to 74.5°W, with a horizontal resolution of 500 m and a vertical resolution of 10 m. Turner angles were computed using the TEOS-10 toolbox routines (McDougall & Barker, 2011; Feistel, 2012).

Note 4: Estimating ε and χ dissipation rates

Based on microstructure measurements, the turbulent mixing –associated with horizontal velocity vertical shear instabilities– is usually determined through the Turbulent Kinetic Energy (TKE) dissipation rate (ε) (Gregg et al., 2018; Osborn, 1980), which, in an isotropic medium is given by

$$\varepsilon = \frac{15}{2}\nu\overline{\left(\frac{\partial u}{\partial z}\right)^2} = \frac{15}{2}\nu\int_0^\infty \psi(k)dk, \tag{S5}$$

where ψ is the vertical velocity shear spectrum, ν is the kinematic viscosity of seawater ($\sim 1 \times 10^{-6} m^2 s^{-1}$) and k the wavenumber associated with turbulent eddy size.

Since the sampling rate of the instruments used to measure turbulence in the ocean (e.g., *VMP 250IR, Rockland Scientific Inc.*) is constant in time (and not in space), the wavenumber spectrum is derived from the frequency spectrum. The frequency spectrum is converted to the wavenumber spectrum by considering the 'Taylor frozen field hypothesis', where the time series can be converted to a spatial one by using

$$g(t) \rightarrow g(z = Wt), \tag{S6}$$

where W is the profiling velocity. Then, the wavenumber spectrum and the frequency spectrum are related by

$$\psi(k) = W\phi(f) \tag{S7}$$

To process the data from the VMP-250 we have used the toolbox provided for *Rockland Scientific Inc. ODAS*. The TKE dissipation rate was computed using 8 s segments with a 50% overlap between successive estimates. The spectrum was calculated in 4 s intervals, which at a nominal fall rate velocity of ~0.7 m/s is equivalent to estimates every ~2.8 m ε depth, see Lueck (2016) for details.

The response of shear sensors is limited by their size (rather than their response time). Larger eddies compared to the sensor diameter are fully resolved, while the measurement of smaller eddies is attenuated by the size of the sensor surface. The spectral response is about one half at a wavenumber of 48 cycles per meter (cpm) (Macoun & Lueck, 2004) and follows the equation

$$H^2(k) = \frac{1}{1 + (k/48)^2}, \tag{S8}$$

where H^2 represents the spectrum reduction function due to spatial averaging. All spectra obtained were corrected using (S8) up to wavenumbers of 150cpm.

The thermal variance dissipation rate (χ) has traditionally been estimated using the temperature gradient spectrum by two methods: integrating over the wavenumbers of the spectrum directly (e.g., Ruddick et al., 2000; Sherman & Davis, 1995) or by Batchelor spectrum fitting techniques for very high wavenumbers (e.g., Luketina & Imberger, 2001; Merrifield et al., 2016), however, the measurement of χ has historically been challenging, particularly in energetic flows since high wavenumbers of temperature gradients are not well resolved with current technology due to the poor response of the sensor commonly used for these measurements (FP07) at high frequencies (e.g., Sommer et al., 2013).

In this work we used the methodology described by Bluteau et al., 2017 where they describe a method that determines χ by spectral fitting to the inertial-convective (IC) subrange of the temperature gradient spectra, in conjunction with direct integration of the temperature spectrum for less energetic moments, the latter was used in this work.

The thermal variance dissipation rate can be estimated from the turbulent temperature gradient (Oakey, 1982), which within an isotropic medium is given by

$$\chi_I = 6\kappa \overline{\left(\frac{\partial T'}{\partial x_3}\right)^2} = 6\kappa \int_0^\infty \phi_{\partial T/\partial x_3}(k)dk, \tag{S9}$$

where κ is the molecular heat diffusivity.

The technique to obtain the temperature spectrum was the same as detailed above for ε, except that the frequency spectrum obtained was corrected for the sensor response using

$$H(f) = \frac{1}{(1 + (2\pi\tau f)^2)^2}, \tag{S10}$$

with $\tau = \tau_o(\overline{u_3}/u_o)^{-1/2}$, , where $\tau_o = 4.1 \times 10^{-3}$, $u_o = 1ms^{-1}$ and $\overline{u_3}$ the instrument fall rate velocity (Bluteau et al., 2017). The frequency spectrum was converted to the wavenumber spectrum analogously using equation (S7).

Both measurements, CTD and microprofiler are constant in time (and not in space), leading to independent profile measurements not necessarily coinciding at the same depth (pressure) levels, to correct for this all temperature, salinity, density, ε, and χ profiles were linearly interpolated every 2 m (from about 20 m to the maximum depth of each profile; see Figure 2 in the main text).

Note 5: Salt finger and diapycnal diffusivity

According to St. Laurent & Schmitt (1999), the parameter space in which salt-finger instabilities develop most efficiently is defined by the conditions: $sfs = [1 < R_\rho < 2, Ri > 1]$, where R_ρ is the density ratio and Ri is the gradient Richardson number.

Local estimates of R_ρ were derived from conservative temperature and absolute salinity profiles collected by the CTD sensors integrated into the VMP-250. These profiles were vertically interpolated to a resolution of 2 m. Ri profiles were computed for each VMP downcast for which independent but simultaneously ADCP velocity measurements were available (see Figure 6, main text).

To synchronize the ADCP data with the VMP profiles, horizontal current measurements were first averaged over 2-minute intervals. A 31-point moving mean was applied in the time domain to filter out high-frequency variability, followed by a 5-point moving average in the vertical. A representative current profile was then computed by averaging over the duration of each VMP-250 fall (typically 10–15 minutes). These profiles were linearly interpolated to a vertical resolution of 2 m, over which the vertical shear components ($\partial U/\partial z$ and $\partial V/\partial z$) were calculated. Ri was then estimated using the computed shear and squared buoyancy frequency (N^2) from the VMP-CTD data.

In July 2021 and October 2022, gradient Richardson numbers exceeded unity in 70% and 81% of cases, respectively, where ADCP data were available. Based on these results, we assumed Ri > 1 for all observations in January 2020, despite the absence of direct ADCP measurements during that campaign. This assumption may lead to an overestimation of Pf (salt-finger occurrence fraction) by approximately 10%, based on comparison with the 2021 and 2022 dataset.

The sfs were assessed within seven potential density anomaly (σ_t) intervals. These intervals were selected to capture the vertical transitions between distinct water masses in the study region, with finer vertical resolution near the salinity maximum in the core of the OMZ (see Figure 4, main text). This approach enabled estimation of the relative contributions of salt-finger mixing (Pf) and mechanical turbulence (Pt) within each interval.

The ensemble averages $\langle \varepsilon \rangle$ and $\langle \chi \rangle$, used in the calculation of mechanical turbulence and salt-finger-related diffusivities, respectively, were computed according to Equations (S5) and (S9). These represent mean dissipation rates derived from all observations falling within each density interval. The mean values $\bar{N}^2$, $\bar{\Theta}_z^2$, $\bar{S}_z^2$ and $\bar{R}_\rho$ were estimated from a least-squares slope fitting inside each of the 7 density intervals.

The diffusivities associated with mechanical turbulence (K_{st}) and salt fingers (K_{sf}), were computed using equations (1) and (3) (in the main text). Thus, the net diapycnal diffusivity (K) was calculated using equation (4) (main text) for each density interval.

Figure S1a. CTD-O profiles for January 2020. Conservative temperature (°C; black line), absolute salinity (g kg⁻¹; red line), potential density anomaly (kg m⁻³; blue line; with reference pressure 0 m), and dissolved oxygen ($\mu mol\ L^{-1}$; magenta line). Panels A and B correspond to the shaded sections in the January 2020 profiles and seek to highlight the impact that the salt fingers would be generating in the density profile where small steps can be seen.

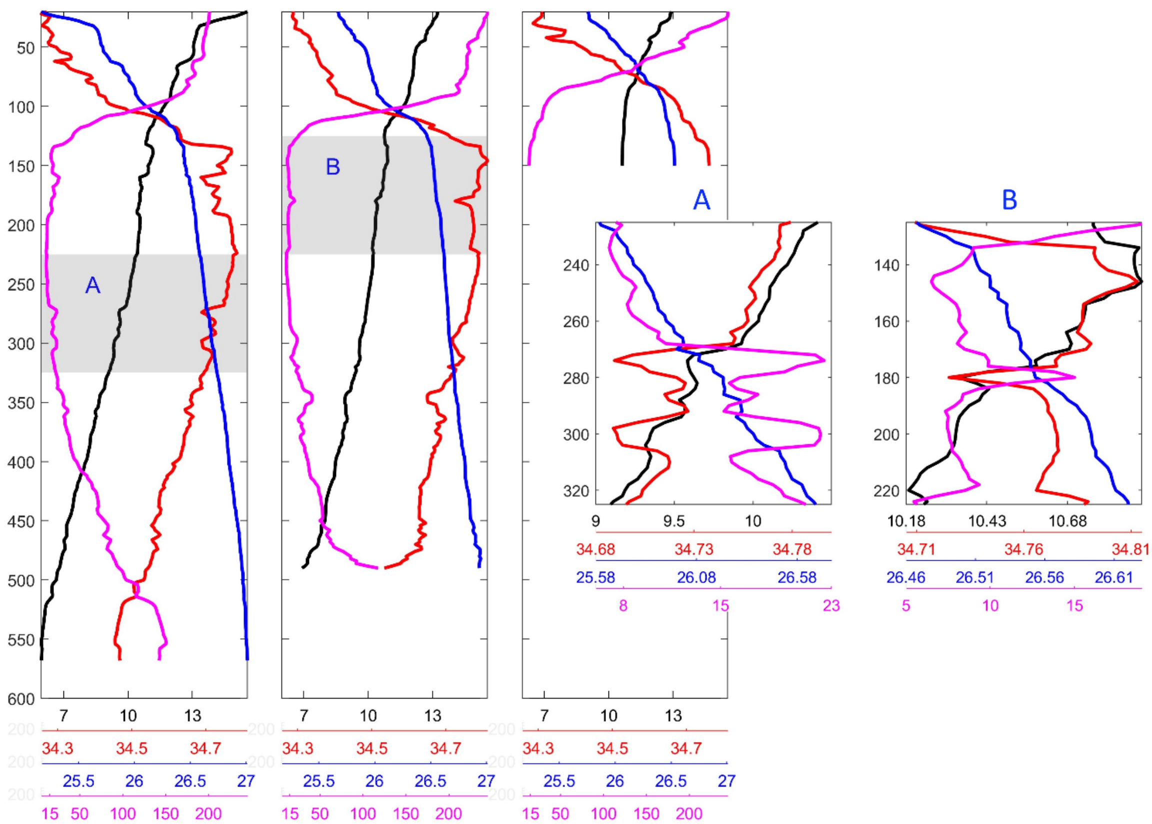

Figure S1b. Same as Figure S1a for July 2021

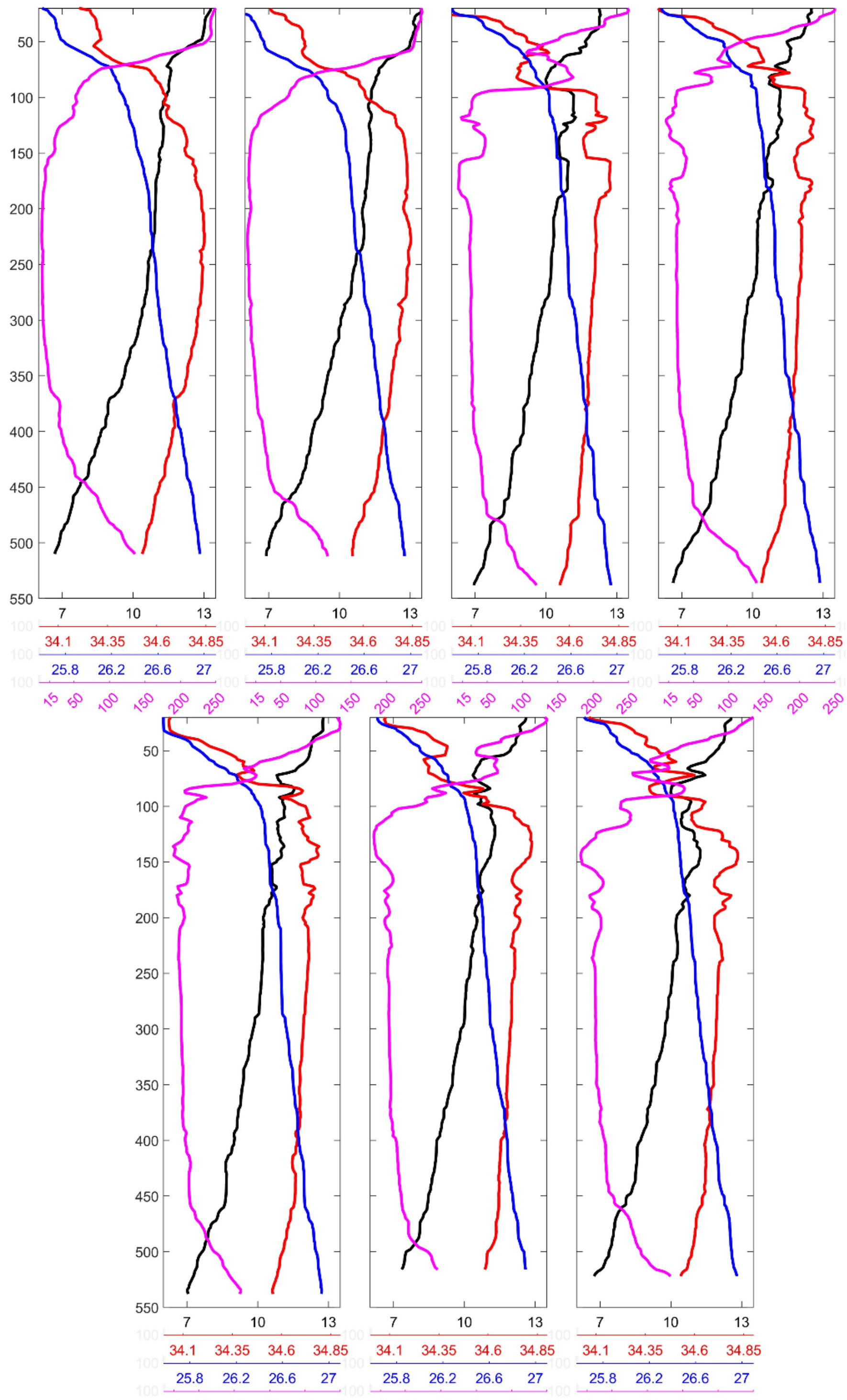

Figure S1c. Same as Figure S1a for October 2022

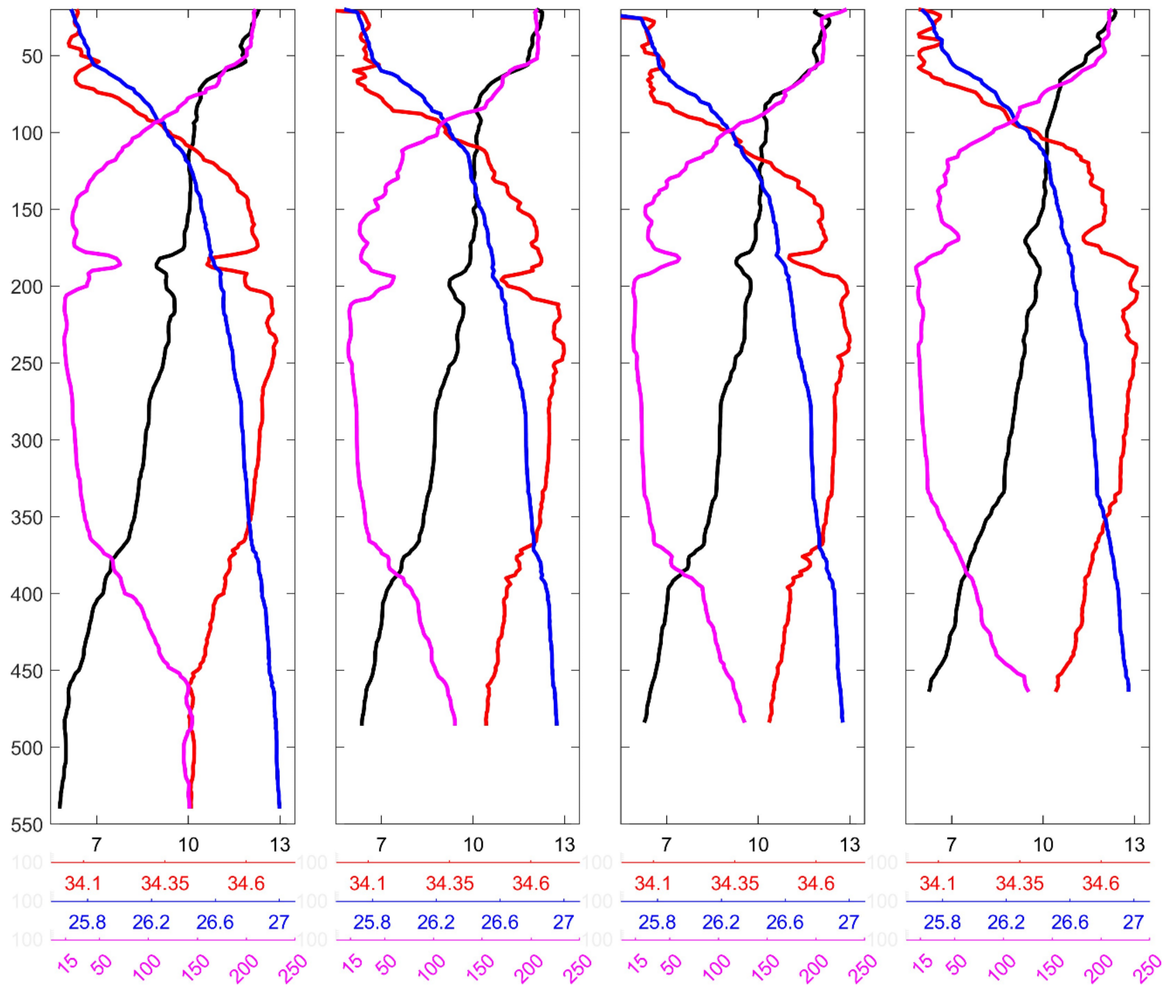

Figure S2. Map of historical (1980-2022) CTD data from WOD used to determine the mean conditions in terms of temperature, salinity, oxygen, and Turner angle for the OMZs of the Perú-Chile (a) (see Figure 1e), California (b), Benguela (c), and Canarias (d) Eastern Boundary Systems. The blue (red) dots indicate available CTD (CTD-O) measurements in the zone.

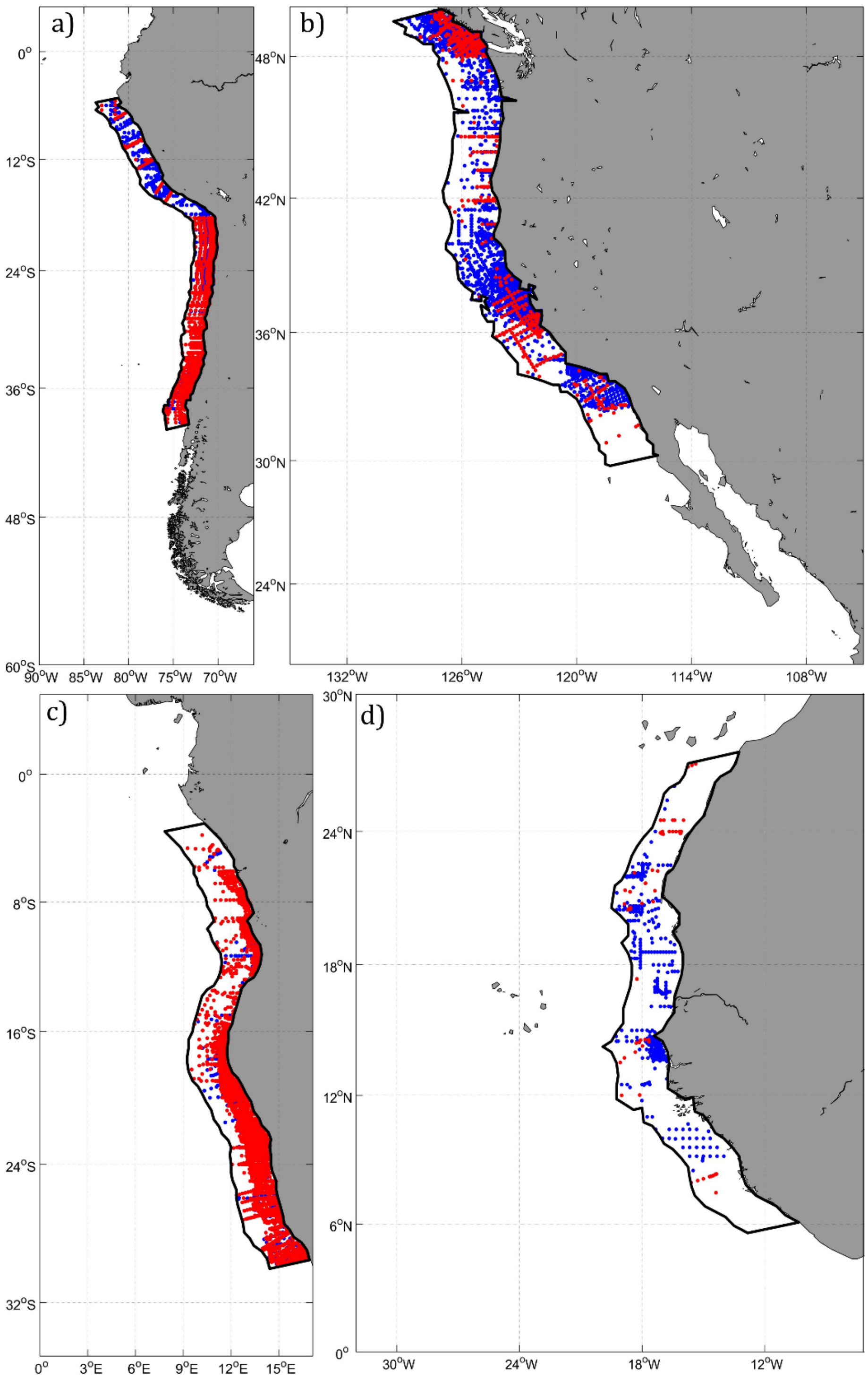

Figure S3. Same as Figure 1e for California (a), Benguela (b) and Canarias (c) Eastern Boundary Systems.

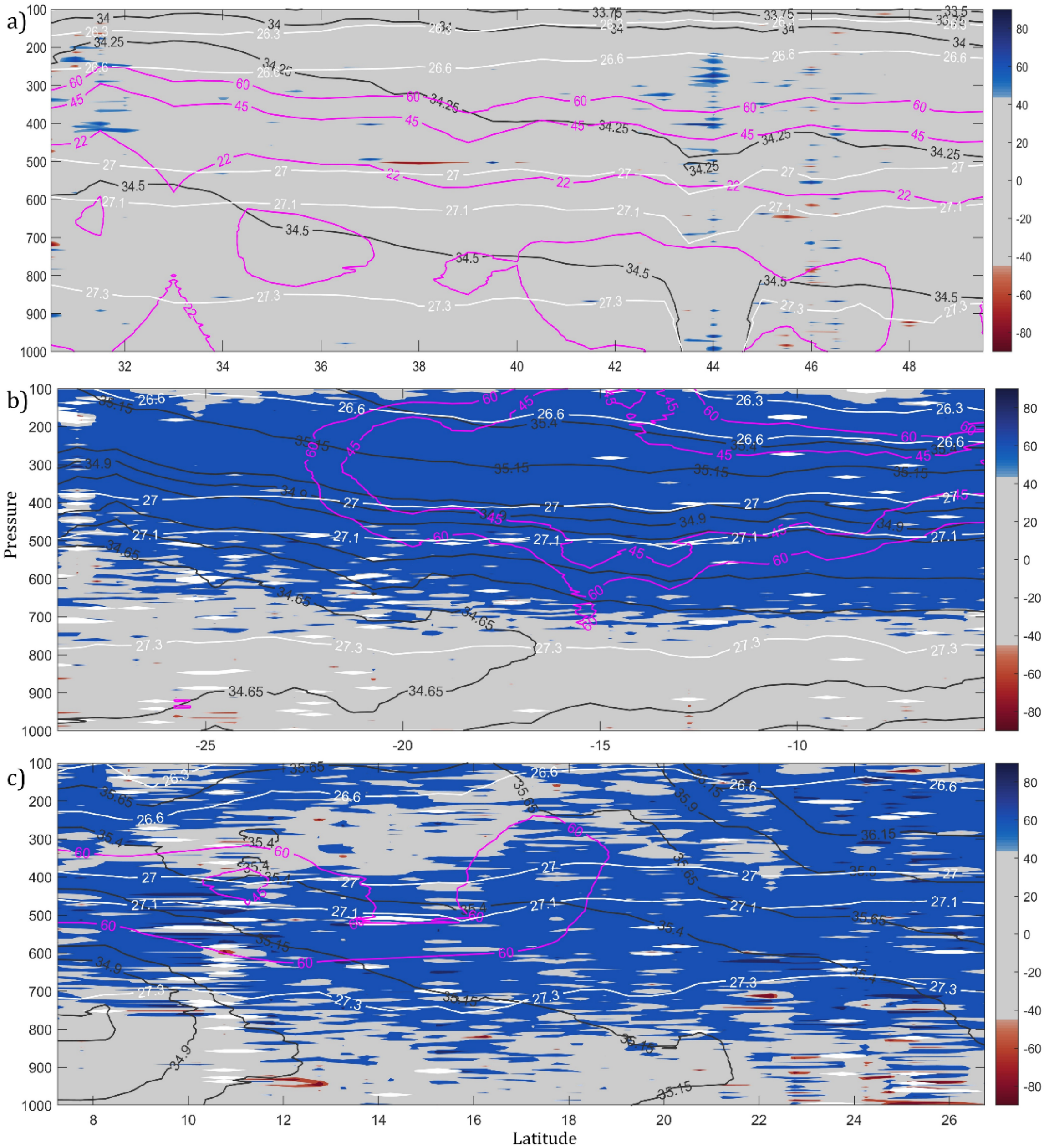

Figure S4a. Cross section from a time series of glider data in the OMZ off Central Chile. The outward (left) and inward (right) trajectory of the underwater glider is shown. From top to bottom: Conservative temperature (°C), absolute salinity (g kg^{-1}), dissolved oxygen ($\mathbf{\mu mol\ L^{-1}}$) and Turner angle (°) for the year 2010.

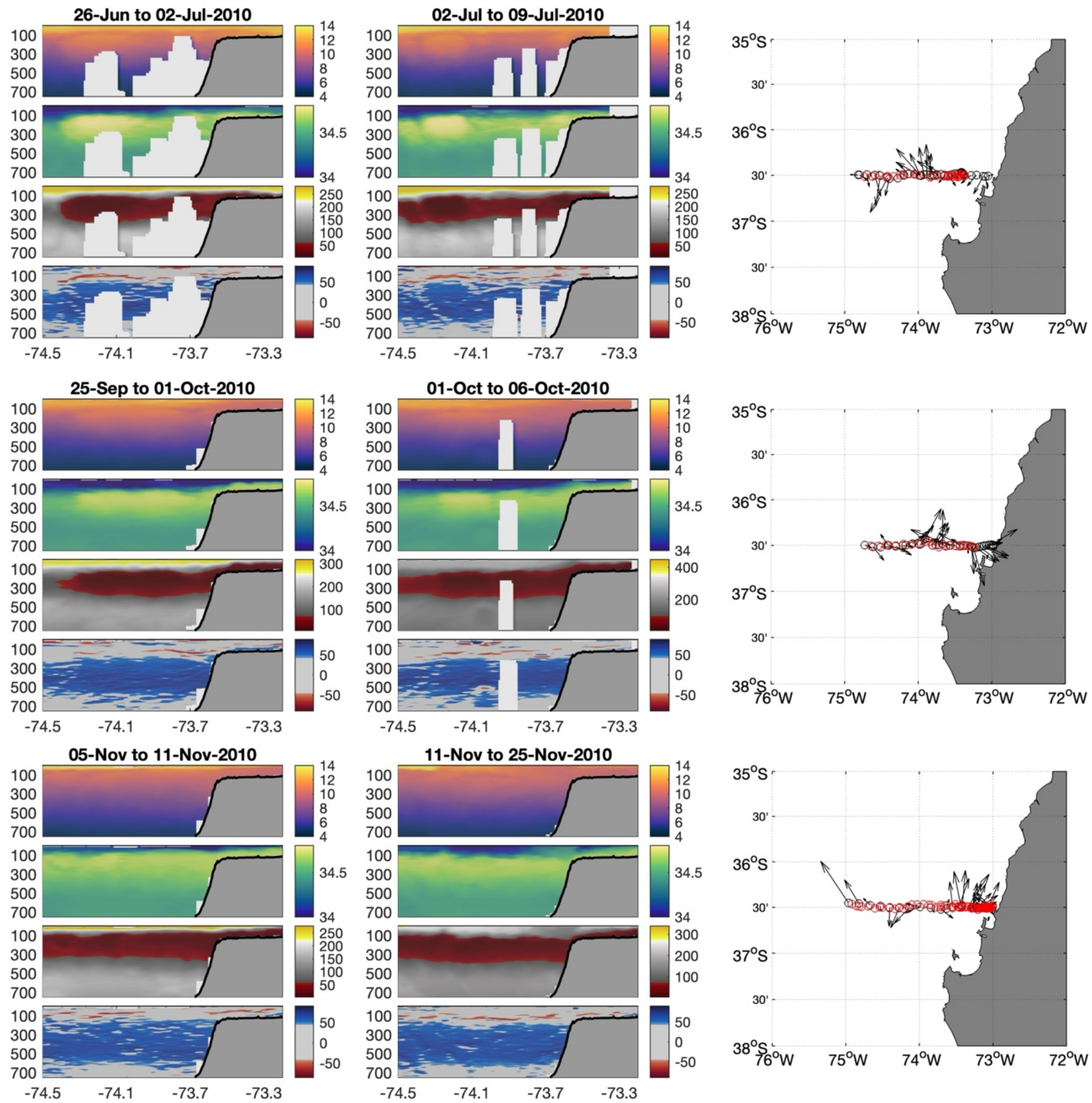

Figure S4b. Same as Figure 4a for 2011.

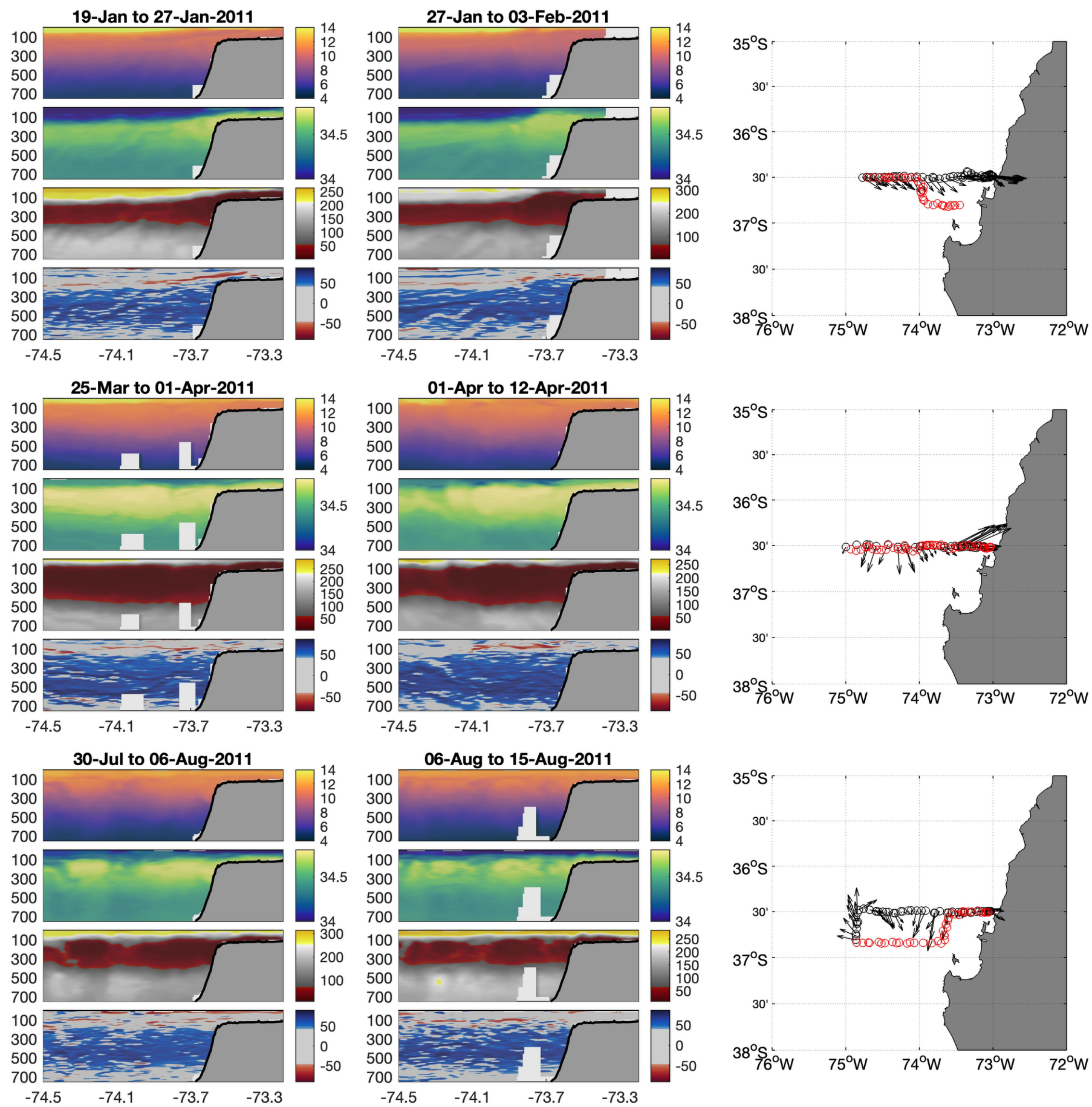

Figure S4c. Same as Figure 4a for 2012.